NORSAR Scientific Report No. 1-2006

Semiannual Technical Summary

1 July - 31 December 2005

Frode Ringdal (ed.)

Kjeller, January 2006

6.4 Seismic/Infrasonic Processing: Case Study of explosions in north Finland

6.4.1 Introduction

Each year between mid-August and mid-September, a series of explosions in the north of Finland is recorded by the stations of the Finnish national seismograph network and also by the seismic arrays in northern Fennoscandia and NW Russia. Based upon event locations given in the seismic bulletin of the University of Helsinki, the geographical coordinates of the explosion site are assumed to be approximately 68.00°N and 25.96°E. The explosions are carried out by the Finnish military in order to destroy outdated ammunition and are easily identified from the automatic seismic bulletins at NORSAR for several reasons. Firstly, they are always detected with a high SNR on the ARCES array, secondly they register very stable azimuth estimates on the detection lists, and thirdly they take place at very characteristic times of day (the origin time indicated by the seismic observations almost invariably falls within a few seconds of a full hour, or half-hour in the middle of the day). A preliminary list of candidate events was obtained by scanning the GBF (Kværna and Ringdal, 1989) automatic detection lists[1] for events which appeared to come from the correct region at appropriate times of day. A typical example is shown in Figure 6.4.1.

NORTHERN LAPLAND FINLAND

Origin time	Lat	Lon	Azres	Timres	Wres	Nphase	Ntot	Nsta	Netmag
2005-242:11.00.06.0	68.23	26.58	5.61	0.87	2.27	4	9	3	1.37

Sta	Dist	Az	Ph	Time	Tres	Azim	Ares	Vel	Snr	Amp	Freq	Fkq	Pol	Arid	Mag
ARC	151.7	163.0	p	11.00.28.3		177.1	14.1	6.1	128.8	615.0	5.36	1		530183	
ARC	151.7	163.0	Pg	11.00.30.3	-0.1	175.8	12.8	8.6	12.8	587.5	5.73	2		530190	
ARC	151.7	163.0	p	11.00.34.6		169.5	6.5	7.2	5.1	95.9	4.63	3		530197	
ARC	151.7	163.0	Lg	11.00.51.8	2.5	171.2	8.2	4.5	30.4	1486.9	4.77	2		530213	1.40
APA	278.5	287.6	Pn	11.00.47.2	-0.5	286.7	-0.9	9.4	4.2	236.4	5.00	1		530285	
APA	278.5	287.6	p	11.00.53.1		274.2	-13.4	8.6	5.8	268.1	4.00	1		530287	
APA	278.5	287.6	s	11.01.21.7		283.2	-4.4	4.1	8.7	566.5	6.09	2	-2	530289	1.34
APA	278.5	287.6	Lg	11.01.25.9	0.4	287.1	-0.5	3.2	4.4	426.7	4.89	3		530290	1.33
SPI	1155.1	158.5	p	11.02.45.7		166.2	7.7	7.0	7.6	287.1	6.01	1	1	535309	

Fig. 6.4.1. Automatic event location estimate from the GBF list http://www.norsar.no/NDC/bulletins/gbf/2005/GBF05242.html The event is characterised by a high SNR for the P- phase at the ARCES array, an S-P time of approximately 20 seconds for ARCES, and a backazimuth from ARCES of ~177°. The location estimate incorporates detections from the ARCES and Apatity arrays.

Between 2001 and 2005, a total of 108 events were found which appeared to fit the general attributes of explosions from this site; the GBF location estimates for these events are displayed in Figure 6.4.2. These fully automatic estimates display a somewhat surprisingly large geographical spread and, assuming that these events are in fact essentially co-located, the origin times will be correspondingly spurious. Before we proceed in attempting to detect and analyse infrasound signals produced from these explosions, we must first confirm that all of our candidate events are in fact from essentially the same location and then obtain the best possible origin time for each event.

1. See http://www.norsar.no/NDC/bulletins/gbf/

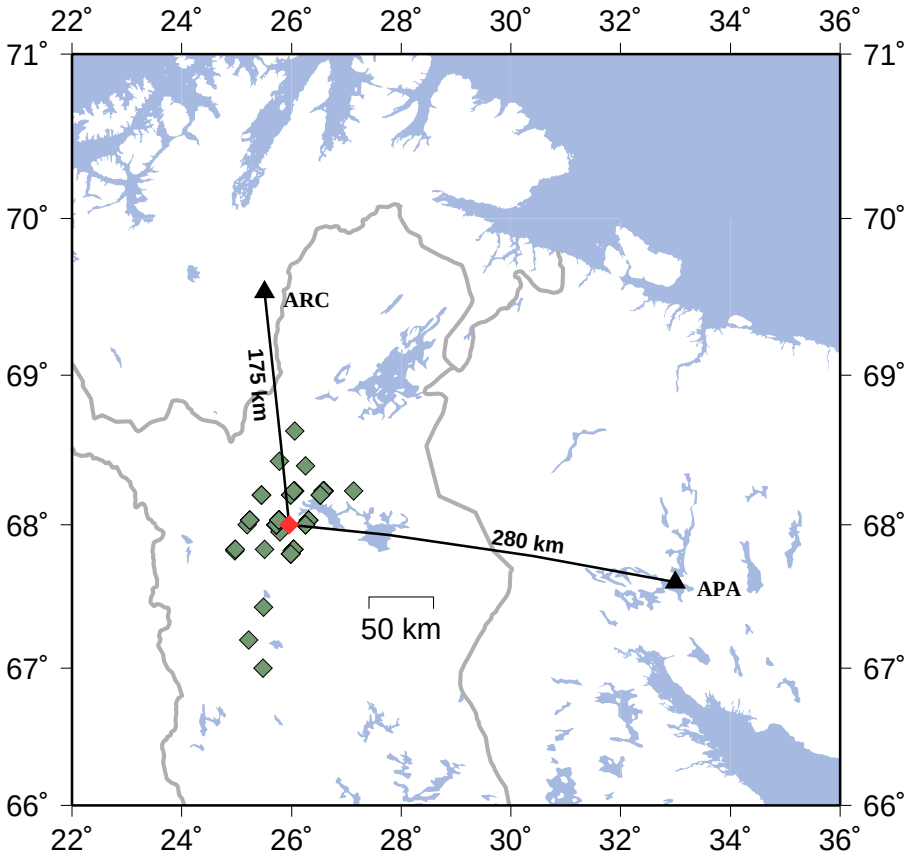

Fig. 6.4.2. Estimated location of the explosion site (orange diamond) in relation to the seismic arrays ARCES and Apatity together with the GBF fully automatic location estimates for 108 candidate events between August 2001 and September 2005 (green diamonds). The regular pattern of event location estimates is due to the fixed-grid trial epicenter procedure employed by the GBF.

6.4.2 Estimation of origin time for the explosions

It has been demonstrated by Gibbons et al. (2005) and Kværna et al. (2005) that far better location estimates can be obtained using one or more regional arrays by applying parameters which have been carefully calibrated for events confirmed to have taken place previously at a site of interest. However, the waveform similarity exhibited between these candidate events suggests that a process analogous to that described in Gibbons et al. (2005) may be circumvented in favour of a derivation of origin times based upon waveform similarity alone.

A single event is chosen as a master event (see Figure 6.4.3) from which an arrival time of the initial P-phase is picked manually. The **barey** model (see Schweitzer and Kennett, 2002) is currently deemed to be the best 1-dimensional velocity model for the region concerned and this predicts that an event occurring at 68.00^{o} N and 25.96^{o} E will result in a first arrival (the Pb phase) after 27.60 seconds. The site defined by these coordinates is 175 km from ARCES which is a difficult distance regarding the identification of phase types since Pb, Pg, and Pn are all predicted to arrive within 1.1 seconds of each other. However, if we assume that an event

has an origin time 27.6 seconds prior to the arrival of the first P-phase, the event displayed in Figure 6.4.3 can be assumed to have an origin time of 2005-244:10.30.00.438.

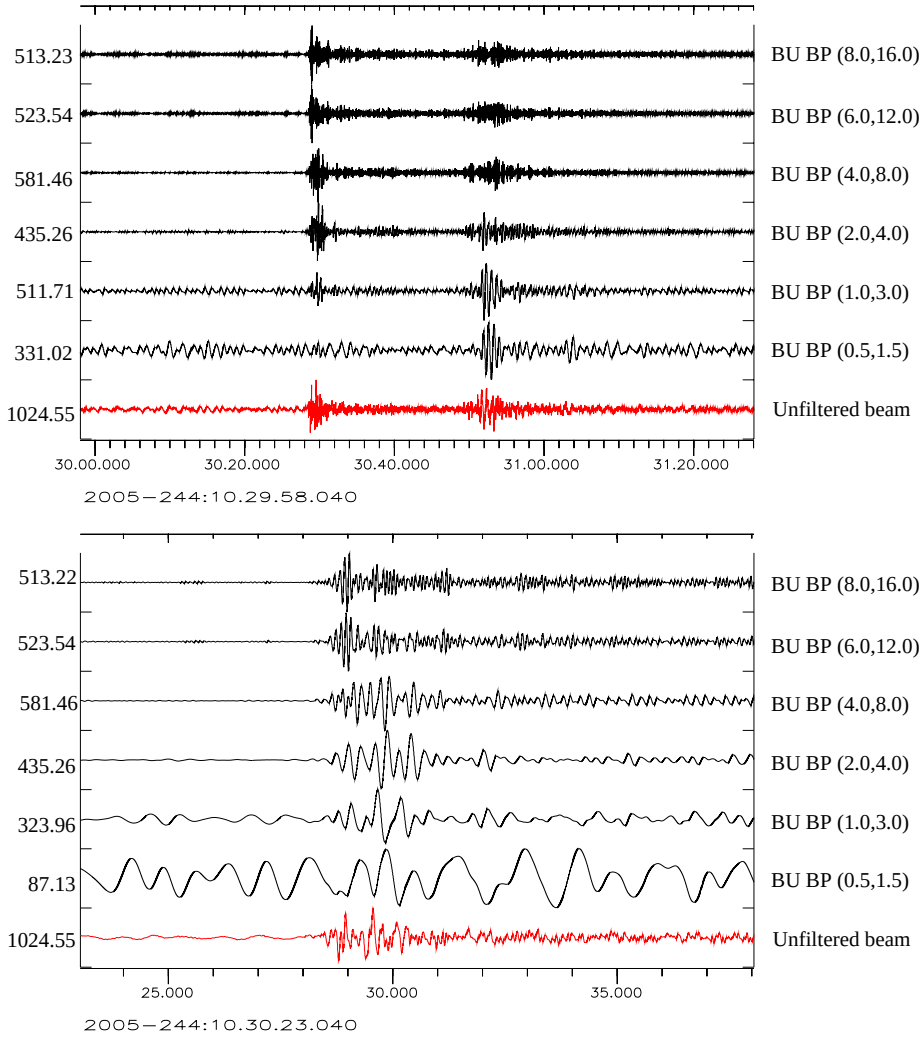

Fig. 6.4.3. Beam at ARCES of signals from an event in Northern Finland at approximately 10:30 GMT on September 1st 2005. The beam is steered with an apparent velocity of 6.72 km/s and a backazimuth of 173^{o}. The onset time of the initial P-arrival is estimated to be 2005-244:10.30.28.380.

We then need to create a waveform template specification for running cross-correlation calculations. We choose to create a template which begins 1.0 seconds prior to the predicted Pg arrival and which ends 40.0 seconds following the predicted Pg arrival. The waveforms are bandpass filtered between 4.0 and 16.0 and the time-series are resampled to 200 Hz. The waveform template is displayed for the ARA0_sz channel in Figure 6.4.4. Each of the short period vertical channels on the ARCES array was provided with the same template specification. The full array waveform template was correlated against data segments for each of the time intervals of interest as has been described in previous reports (e.g. Gibbons and Ringdal, 2004; Gibbons and Ringdal, 2005a,b). A typical cross-correlation detection is displayed in Figure 6.4.5. In fact, every one of the 108 candidate events displayed this degree of waveform similarity; the

lowest correlation coefficient obtained was 0.41 and even this value is significant given the length of the data segment and the high time-bandwidth product.

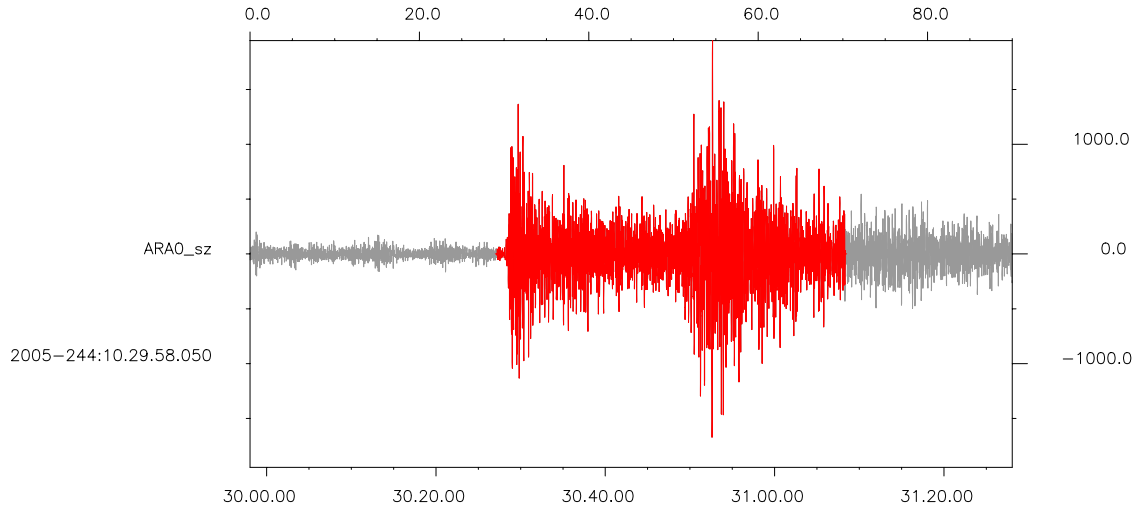

Fig. 6.4.4. Waveform template highlighted in red for the ARA0_sz channel for the 1st September 2005 ammunition destruction explosion in Northern Finland. The waveform is filtered between 4.0 and 16.0 Hz and resampled to 200 Hz.

The high correlation values observed for the event set is a strong indication that the explosions are very closely spaced, although we cannot specify the precise extent of the source area based on these data alone. If we use the 'quarter of the wavelength' criterion of Geller and Mueller (1980), we can, as a first approximation, state that the exlosions probably occurred within an area of less than 1 km in diameter.

That all of these explosions are thereby constrained to have occurred within such a small source region should make this data set a useful benchmark for future improvements to automatic event location algorithms aimed at improving the situation inferred from Figure 6.4.2. The time of maximum cross-correlation is obtained to the highest possible degree of accuracy using a spline interpolation and, by considering the definition of the waveform template relative to the manually read arrival time, we can estimate the origin times of each one of the 108 explosions recorded between August 2001 and September 2005. Since these origin times are all determined from the waveform semblance from event to event, any error in the origin time determination is almost certain to be dominated by error in the measurement of the arrival time, inadequacy of the velocity model, or error in the location of the explosion site. This is to say that the error is essentially identical for each event and that if, for a future explosion, it were possible to obtain an absolute GPS source location measurement and a precise origin time then all of the event origin times could be corrected simultaneously.

For reference, a list of the origin times for all of the events used in the current study is provided in Figure 6.4.6.

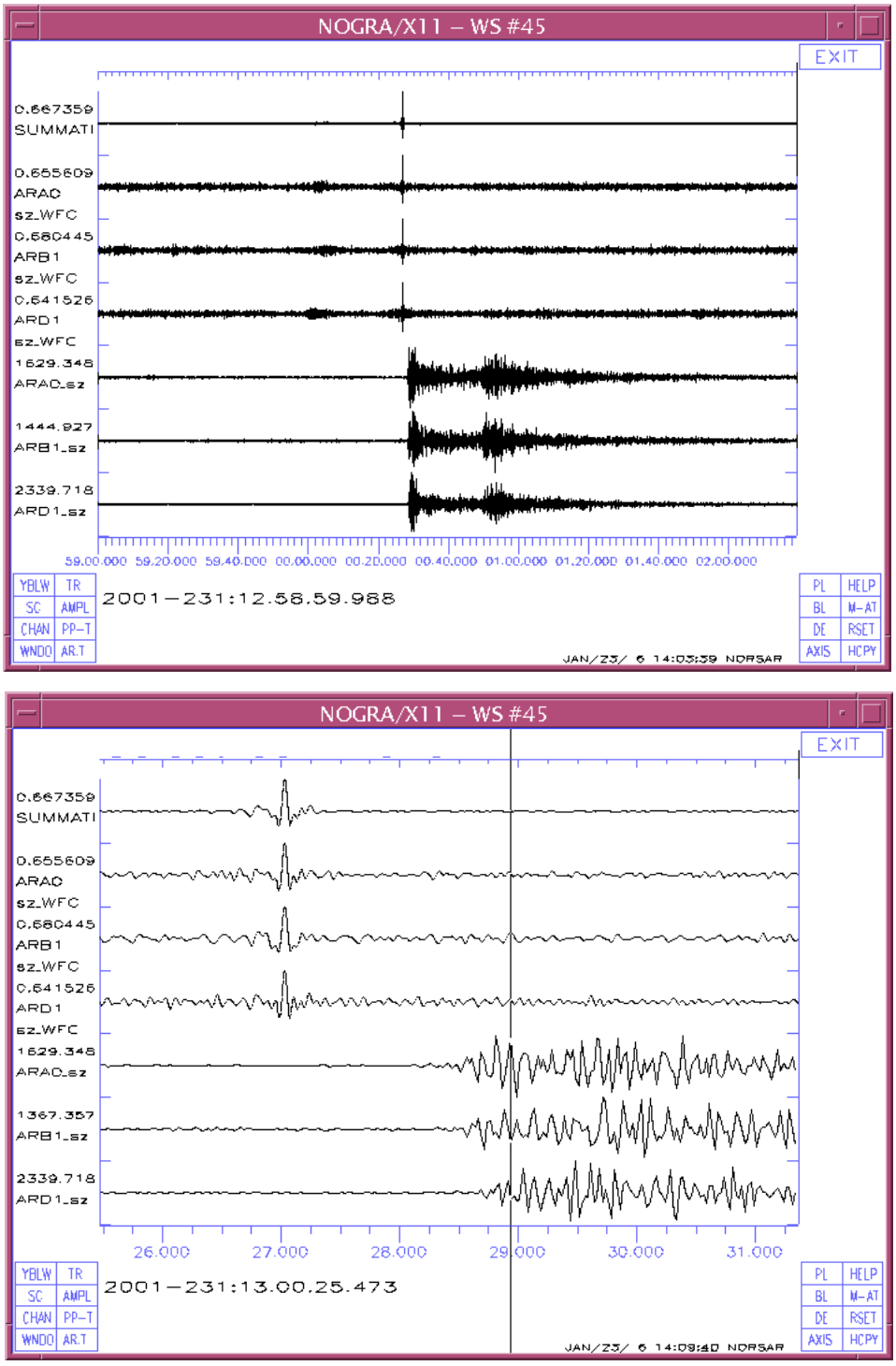

Fig. 6.4.5. Detection by waveform correlation of the August 19th 2001 ammunition destruction explosion in Northern Lapland using the master waveform template displayed in Figure 6.4.4. The 40 second long high-frequency master waveform records a correlation coefficient of 0.66 with the detected waveform, therefore guaranteeing an almost identical source location and type.

2001-228:13.59.59.505	2002-251:13.29.59.938	2004-242:11.30.03.553
2001-229:12.29.58.991	2002-252:11.59.59.483	2004-243:11.00.03.839
2001-230:13.29.58.192	2002-253:11.59.59.947	2004-244:11.00.03.986
2001-231:12.59.59.023	2002-254:11.44.59.738	2004-245:11.30.03.556
2001-232:10.59.59.045	2002-255:10.44.59.803	2004-246:11.00.00.846
2001-233:14.29.58.501	2002-256:10.44.59.615	2004-247:10.30.00.039
2001-234:11.29.59.331	2002-257:10.00.00.387	2004-248:10.00.00.883
2001-235:11.59.59.649	2002-258:10.00.00.087	2004-249:10.59.59.905
2001-236:11.29.59.104	2002-259:11.00.00.112	2004-250:10.00.00.207
2001-237:12.59.56.807	2002-260:10.14.59.787	2004-251:10.00.00.301
2001-238:11.59.56.607	2003-233:12.00.01.685	2004-252:10.30.01.126
2001-239:15.59.56.761	2003-234:11.00.01.756	2004-253:09.00.01.088
2001-240:13.29.56.924	2003-235:11.00.00.283	2004-254:09.00.00.480
2001-241:13.29.56.093	2003-236:10.30.00.027	2004-255:10.00.00.684
2001-242:12.44.56.485	2003-237:10.30.00.185	2004-256:08.59.59.571
2001-243:12.44.56.390	2003-238:11.59.59.930	2004-257:09.29.58.714
2001-244:12.29.56.414	2003-239:09.30.00.915	2004-258:09.00.01.861
2001-245:12.14.56.175	2003-240:10.59.59.804	2005-236:12.00.03.287
2001-246:12.59.59.983	2003-241:10.29.59.778	2005-237:11.00.03.265
2001-247:12.44.59.496	2003-242:10.29.59.588	2005-238:11.00.01.462
2001-248:11.44.59.142	2003-243:09.59.59.906	2005-239:10.00.02.689
2001-249:11.45.00.103	2003-244:11.59.59.408	2005-240:10.59.59.776
2001-250:11.59.56.659	2003-245:11.29.59.139	2005-241:10.59.59.828
2001-251:11.59.57.022	2003-246:10.44.58.987	2005-242:10.59.59.449
2001-252:10.29.56.870	2003-247:09.59.58.642	2005-243:11.59.59.870
2001-254:12.44.55.638	2003-248:09.59.58.486	2005-244:10.29.59.068
2002-241:13.29.59.647	2003-249:10.29.58.397	2005-245:10.59.59.022
2002-242:13.29.59.542	2003-250:11.29.58.247	2005-246:10.59.59.647
2002-243:13.30.00.118	2003-251:09.59.58.067	2005-247:11.00.03.608
2002-244:12.30.00.072	2003-252:10.29.57.973	2005-248:09.00.00.681
2002-245:12.29.59.664	2003-253:10.00.00.555	2005-249:10.00.00.401
2002-246:12.29.59.481	2003-254:11.29.59.883	2005-250:09.45.00.083
2002-247:12.59.59.211	2004-238:13.30.03.333	2005-251:09.45.00.086
2002-248:13.29.58.978	2004-239:12.00.03.518	2005-252:11.30.00.289
2002-249:12.29.58.839	2004-240:11.29.03.564	2005-253:10.45.00.017
2002-250:12.59.58.477	2004-241:11.29.04.079	2005-254:09.59.59.828

Fig. 6.4.6. List of estimated origin times for the 108 events from the Finnish explosion site used in this study.

6.4.3 Data analysis

Ringdal and Schweitzer (2005) presented a case study of seismic and infrasonic recordings of six presumed surface explosions in Pechenga, Russia, near the Norwegian border. The explosions in northern Finland described in this paper have many of the same characteristics, although the infrasonic signals are not as large as those observed for the Pechenga explosions. Nevertheless, the SNR is sufficient to provide slowness estimates at the ARCES array for the seismic signals (in all cases) and for infrasonic signals (in the majority of cases). We will use various subconfigurations of the ARCES array (see Figure 6.4.7) in our further analysis of these signal characteristics.

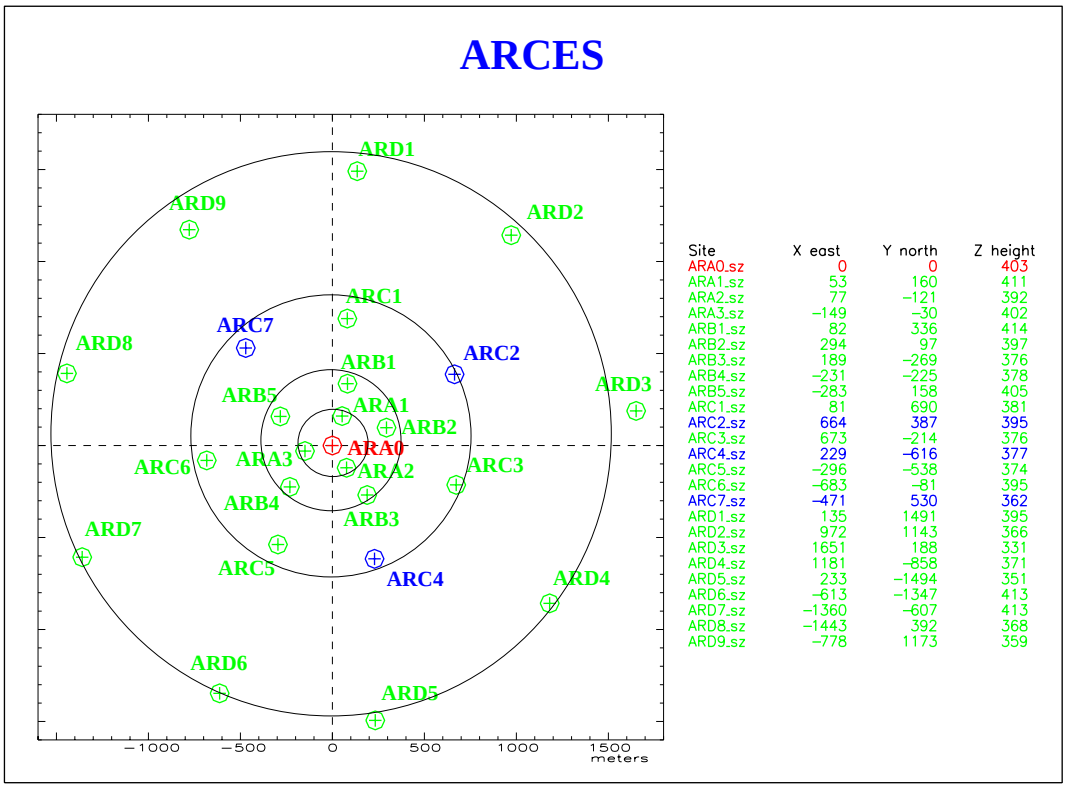

Site	X east	Y north	Z height
ARA0.sz	0	0	403
ARA1.sz	53	160	411
ARA2.sz	77	−121	392
ARA3.sz	−149	−30	402
ARB1.sz	82	336	414
ARB2.sz	294	97	397
ARB3.sz	189	−269	376
ARB4.sz	−231	−225	378
ARB5.sz	−283	158	405
ARC1.sz	81	690	381
ARC2.sz	664	387	395
ARC3.sz	673	−214	376
ARC4.sz	229	−616	377
ARC5.sz	−296	−538	374
ARC6.sz	−683	−81	395
ARC7.sz	−471	530	362
ARD1.sz	135	1491	395
ARD2.sz	972	1143	366
ARD3.sz	1651	188	331
ARD4.sz	1181	−858	371
ARD5.sz	233	−1494	351
ARD6.sz	−613	−1347	413
ARD7.sz	−1360	−607	413
ARD8.sz	−1443	392	368
ARD9.sz	−778	1173	359

Fig. 6.4.7. ARCES array configuration. The four circles correspond to the A, B, C and D-rings as discussed in the text.

Figure 6.4.8 shows an example of such a recording at selected ARCES sensors for one of the explosions. In fact, this is one of the explosions which had the largest infrasound signals; in most cases, the infrasound phase was hardly visible on single sensor traces, even though f-k analysis could nevertheless be carried out.

Thus, this data set of more than 100 surface explosions in almost exactly the same place recorded by the ARCES array provides an excellent opportunity to investigate the stability of slowness estimates, both for the seismic and infrasonic recordings, as presented in the following. We will do such analysis investigating both the effects of filter frequency band, array aperture and number of sensors. In this respect, we will use various sub-configurations of ARCES to simulate array configurations of various diameters and number of sensors.

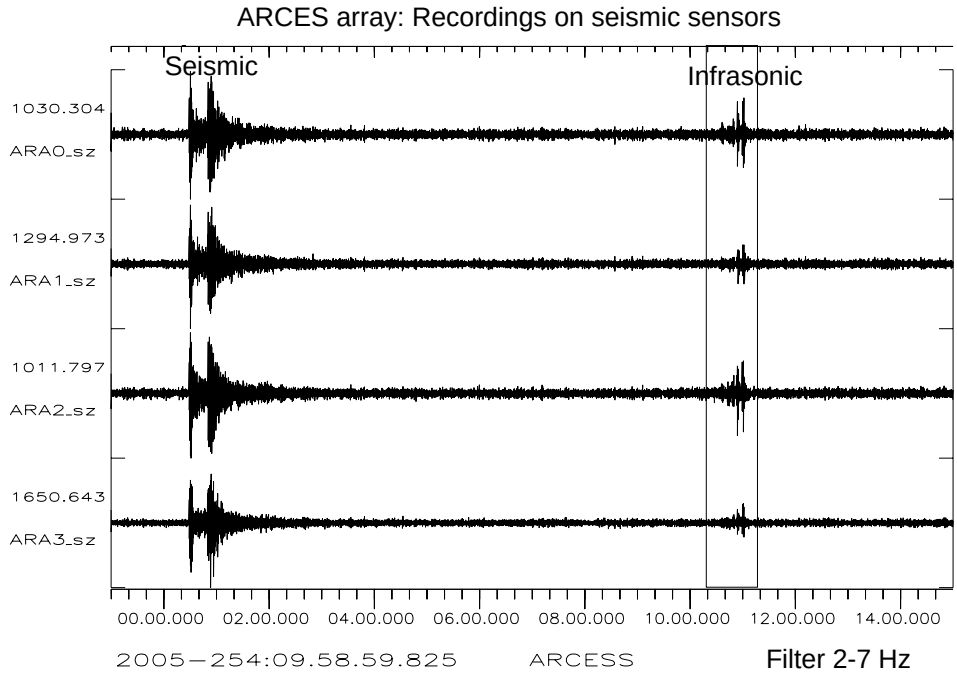

Fig. 6.4.8. ARCES waveforms for one of the explosions discussed in the text (Event 108 in the table). Note the clear recording of both the seismic P and S waves and the infrasonic waves, which appear about 10 minutes later. The 60-second interval used for the infrasonic f-k analysis is marked on the plot.

6.4.4 Seismic P-phases

Figure 6.4.9 shows the ARCES slowness estimates for the 108 events in four different frequency bands. As has been observed by Gibbons et. al. (2005) and Kværna et. al. (2005), such estimates are very stable when fixed frequency bands are applied, and, not surprisingly, this figure confirms this stability. The standard deviation in azimuths is as small as 0.3 degrees for the best filter (3-5 Hz), and is 1 degree or lower for all the filters shown. The average values of the azimuth estimates varies by up to 5 degrees among the filters, and these differences are highly significant in view of the small scatter in each population (The standard deviations of the mean values range from 0.03 to 0.1 degrees).

We note that the length of the f-k window (10 seconds) used in the present study is somewhat longer than the traditional 2-3 seconds used in standard detection processing. This may have provided some increased stability in the slowness estimates, but we have not investigated this question in any detail.

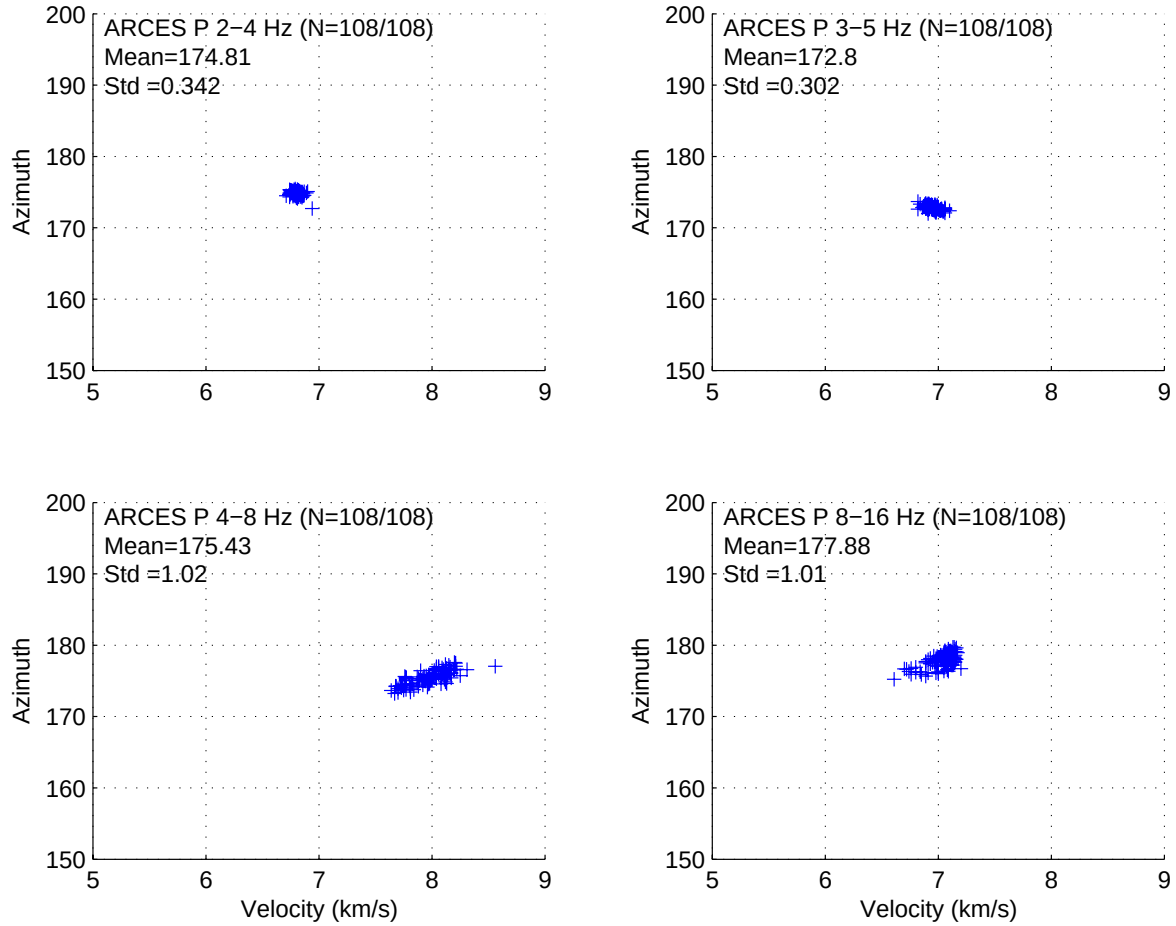

Fig. 6.4.9. Slowness estimates of the 108 events in the data base. The figure corresponds to estimates for the seismic P-phase (25-35 seconds after the event origin time), in four different filter bands. For each filter band, the mean and standard deviation of the azimuth estimates are indicated.

Fig. 6.4.10 shows the ARCES slowness estimates for the event set as a function of various sub-configuration of vertical-component seismometers. These are, in increasing sizes:

- The 4-element A-ring configuration (seismometers A0, A1, A2, A3)
- The 9-element A,B-ring configuration (by adding the seismometers B1-B5)
- The 16-element A,B,C-ring configuration (by adding the seismometers C1-C7)
- The 25-element A,B,C,D-ring configuration (comprising the full ARCES vertical-component array)

As expected, the scatter of the estimates decreases as the array size and number of seismometers increases, and the amount of decrease in the standard deviations is about proportional to the increase in array diameter. Again, we see that the mean azimuth estimates show significant differences among the array configurations, even if we are applying the same bandpass filter (3-5 Hz) throughout.

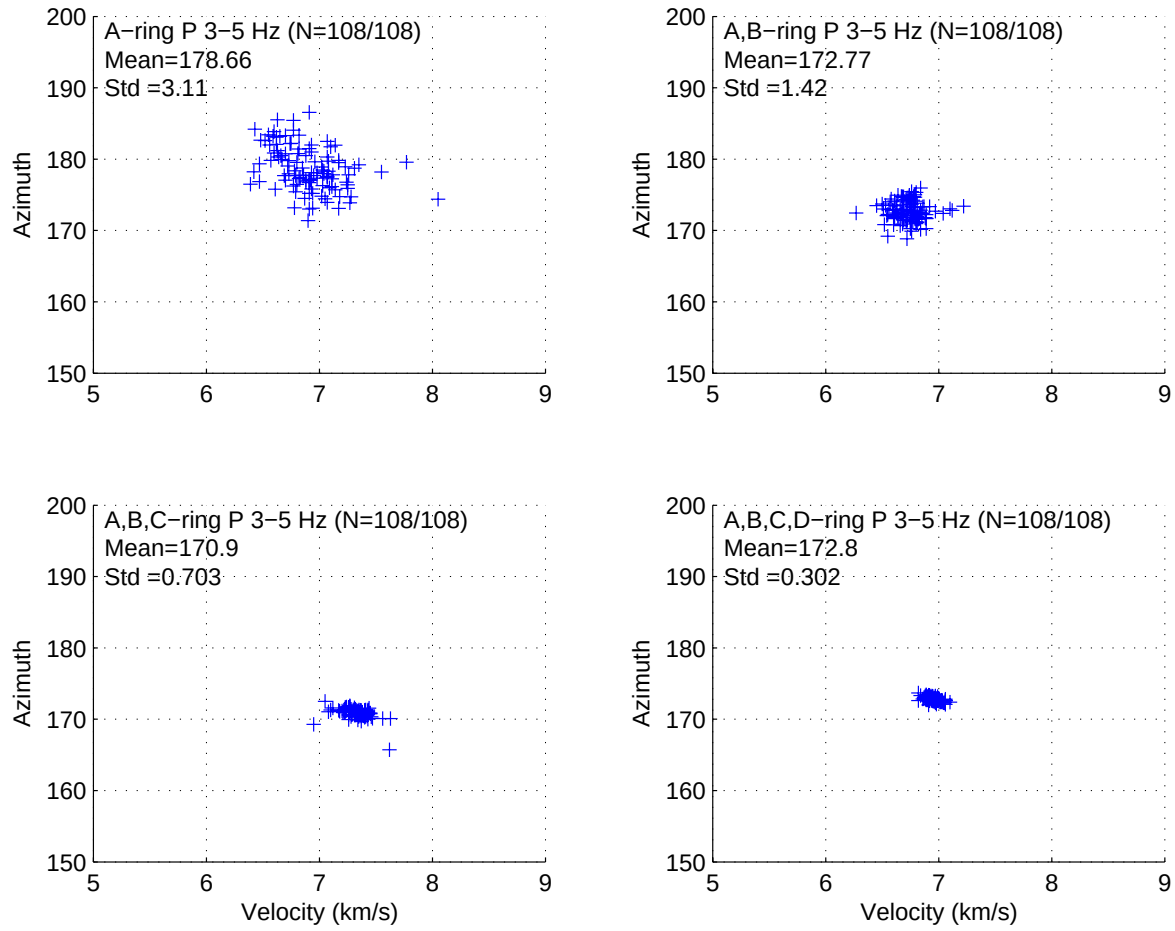

Fig. 6.4.10. Slowness estimates of the 108 events in the data base. The figure corresponds to estimates for the seismic P-phase (25-35 seconds after the event origin time), in the filter band 3-5 Hz. The four subconfigurations are as described in the text. For each subconfiguration, the mean and standard deviation of the azimuth estimates are indicated.

To investigate how much of this observed decrease in scatter is due to array aperture, and how much is due to increased number of seismometers, we made some experiments by selecting only 4 seismometers (in the outermost ring) for each of the four subconfigurations. The results from one such experiment is shown in Figure 6.4.11. The reduction in scatter is quite similar to that in Figure 6.4.10. This indicates that the array aperture is the most important factor in order to obtain variance reduction, whereas the number of sensors in each configuration is not essential in this regard. Nevertheless, an increased number of sensors is useful so as to reduce the possibility of side lobes, and it also adds redundancy which would be important if one or more seismometers malfunction.

An interesting observation is that the adding or removal of a single seismometer in a 4-sensor configuration can have significant effect on the average azimuth (but not much effect on the stability of the estimates). This is an observation that needs to be taken into consideration when doing slowness analysis and location estimation by regional arrays, since the outage of one or more sensors could influence the expected azimuth estimates for any given source region.

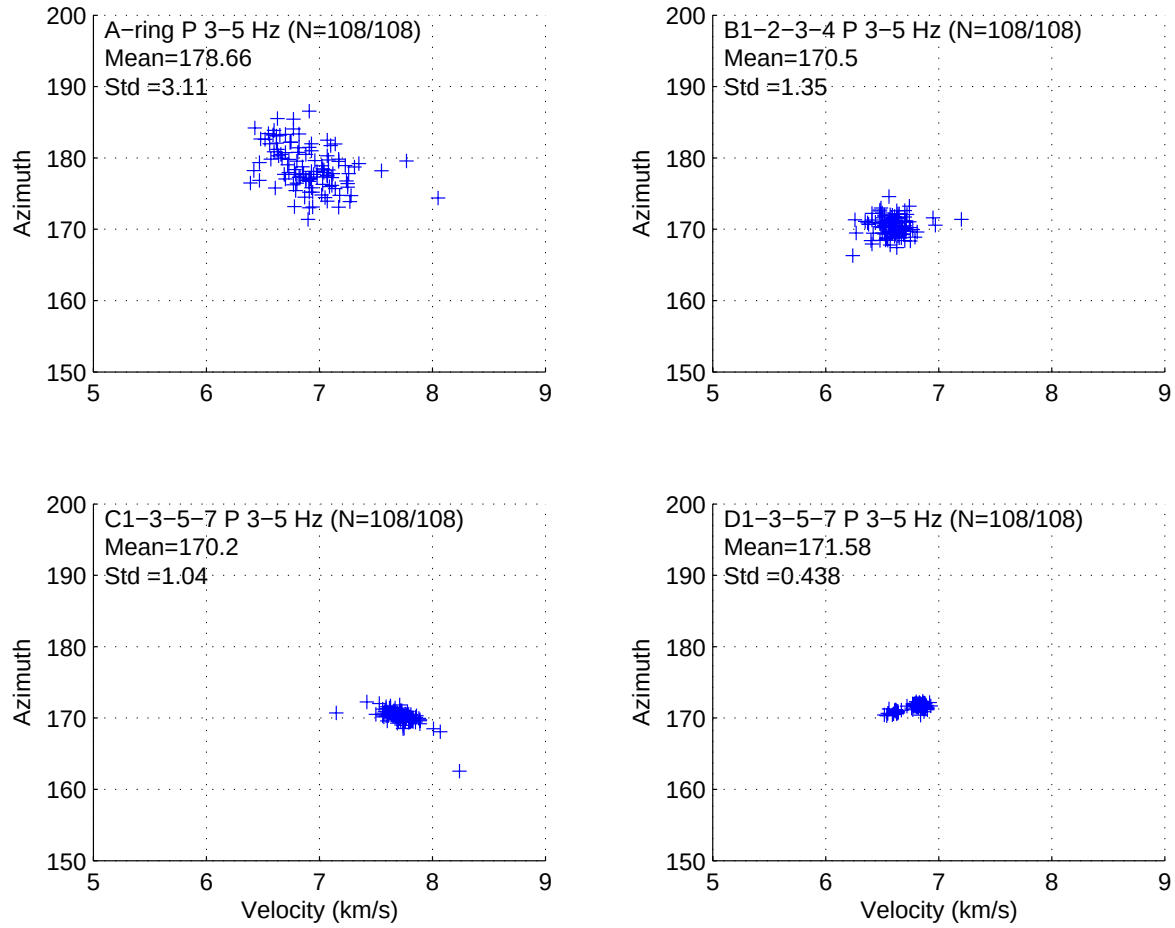

Fig. 6.4.11. Slowness estimates of the 108 events in the data base. The figure corresponds to estimates for the seismic P-phase (25-35 seconds after the event origin time), in the filter band 3-5 Hz. In contrast to Figure 6.4.10, the four subconfigurations now comprise only four seismometers each, as indicated on the plots. Note the similarity to Figure 6.4.10.

6.4.5 Infrasonic waves

In our study of slowness estimates for infrasonic waves recorded at the ARCES seismic array, we have used throughout a 60 second window beginning 620 seconds after the event origin time. Fig. 6.4.12 shows the ARCES slowness estimates for the infrasonic phases (named Ix) as a function of the same sub-configuration of vertical-component seismometers as used in our studies of P-waves described earlier.

In contrast to the P-wave analysis, we were not able to make reliable slowness estimates for the infrasonic phases of all the events. This is mainly due to low infrasonic SNR for a number of the events in the database. This makes a comparison between the performances of different filters and subconfigurations more complicated, and we need to consider both the number of successful estimates and the variance reduction when evaluating the results.

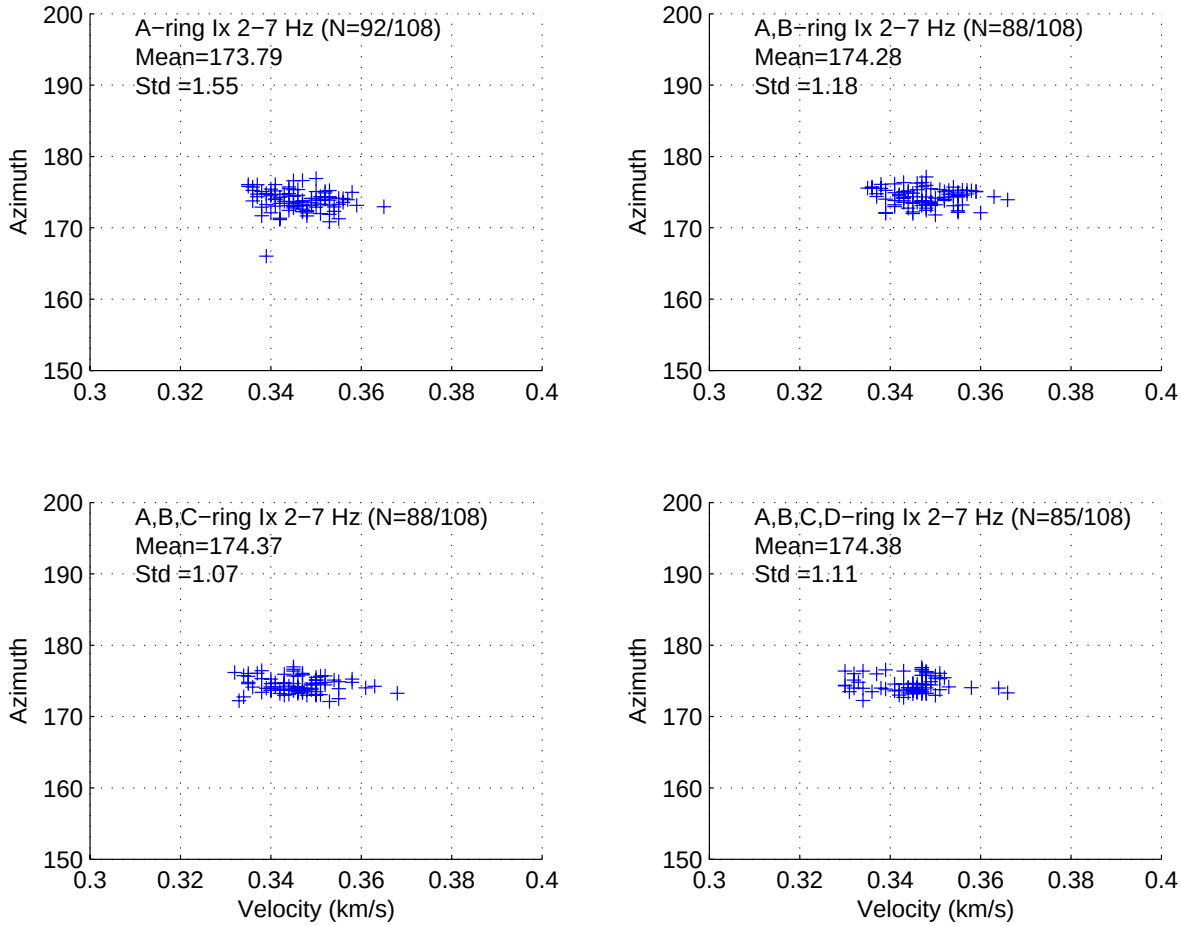

Fig. 6.4.12. Slowness estimates of the 108 events in the data base. The figure corresponds to estimates for the infrasonic phase (620-680 seconds after the event origin time), in the filter band 2-7 Hz. The number of events for which reliable estimates could be made is indicated on each plot. The four subconfigurations are as described in the text. For each subconfiguration, the mean and standard deviation of the azimuth estimates are indicated.

When comparing the results to those obtained for seismic P-waves, we see some interesting differences. For example, we see no significant variance reduction as the array aperture and number of sensors increases. Although there appears to be a slight reduction in the standard deviations, the largest number of successful estimates were in fact made using the smallest configuration. Therefore we consider that there is essentially no difference in the stability of the slowness estimates for these four configurations. It is of course possible that other estimation techniques could show such improvements, but it may also be that the variance in estimates is dominated by factors such as varying atmospheric conditions over the 5 years covered by this study. Another important observation is that the average azimuth values are essentially independent of the subconfiguration chosen. This also contrasts to our observations from seismic P-waves.

In order to study the frequency dependency for infrasonic waves, we found that the SNR of ARCES infrasonic observations were not sufficient to enable us to do a meaningful study. For this purpose, we therefore used data recorded by the microbarographs installed at the Apatity seismic/infrasound array. A description of this array is presented in the paper by Schweitzer et. al. in this issue. Examples of recording and processing of some of these same Finnish

explosions using Apatity infrasonic data have earlier been presented by Vinogradov and Ringdal (2003). In the study presented here, we used a 60 second window starting at 970 seconds after the event origin time for the f-k analysis. Note that we selected for analysis only one of the three infrasonic phases observed at Apatity and desribed in the above publication.

Fig. 6.4.13 shows the Apatity slowness estimates for the infrasonic phase (named Ix) for the events in four different frequency bands. Again, the contrast to the seismic observations is striking. The average azimuth estimates of the infrasonic phases are virtually independent on the frequency band, and there is thus no observable systematic differences in infrasonic slowness estimates as a function of frequency within the bands processed in this study.

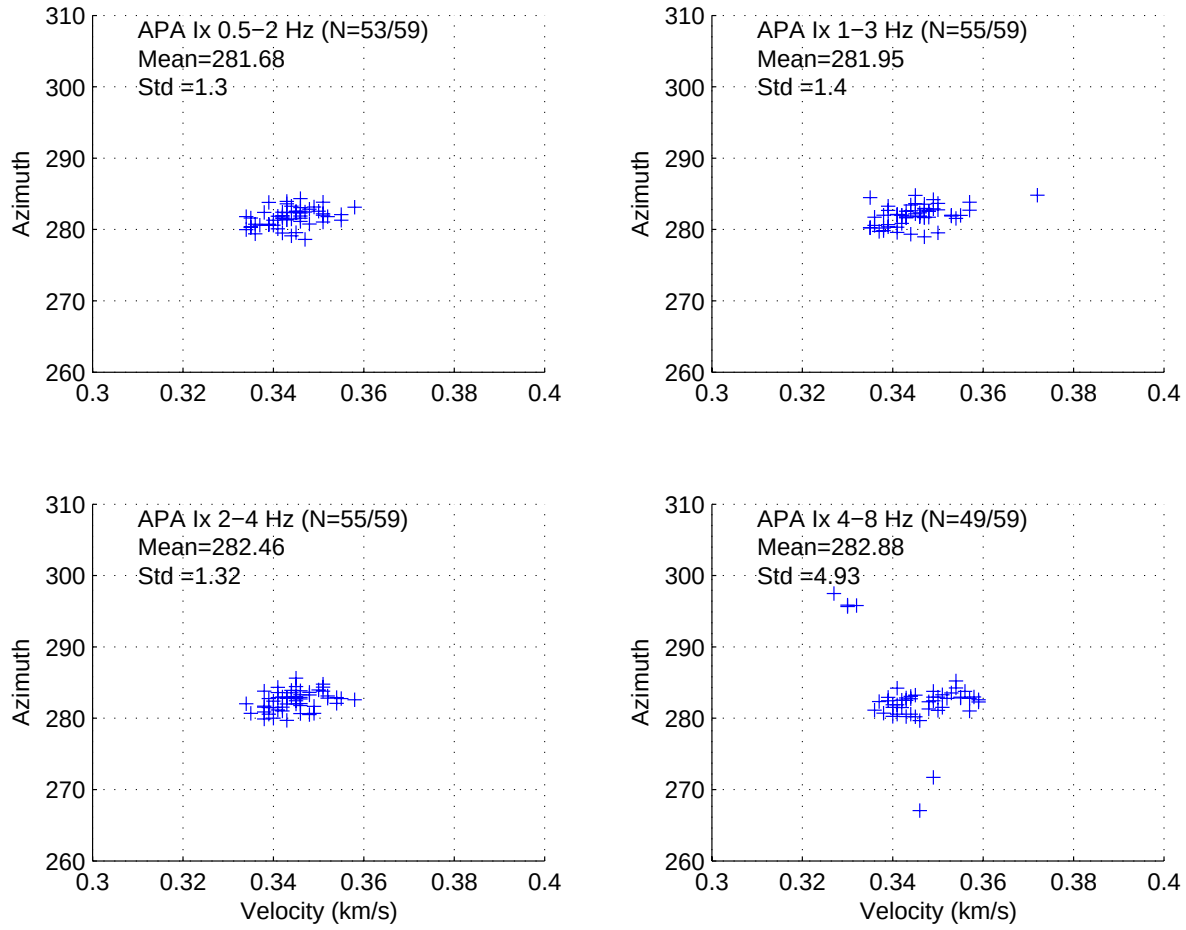

Fig. 6.4.13. Slowness estimates of the 59 events in the data base for which Apatity infrasonic recordings were available. The figure corresponds to estimates for the infrasonic phase (970-1040 seconds after the event origin time), in four different filter bands. The number of events for which reliable estimates could be made is indicated on each plot. For each filter band, the mean and standard deviation of the azimuth estimates are indicated.

6.4.6 Conclusions

We have used waveform cross-correlation to determine very accurate origin times for a data-base of 108 explosions, at a site in northern Finland, presumably carried out for the purpose of destroying old ammunition. The extremely high correlation coefficients observed for this data set indicates that these explosions are all very closely spaced, probably within an area of some hundreds of meters in diameter. This database will be highly valuable for various studies

related to obtaining improved accuracy in detecting and characterizing seismic events using regional array recordings at local distances.

In the present paper, we have used this database to study the stability of slowness estimates for both seismic and infrasonic phases, using ARCES and Apatity array recordings. Our analysis of seismic P-phase observations confirm the stability of fixed-frequency band f-k analysis previously noted e.g. by Gibbons et. al. (2005) and Kværna et. al. (2005). Furthermore, by analyzing various subconfigurations of the ARCES array, we find that the scatter (standard deviation) in the azimuth estimates for the explosions is about inversely proportional to array aperture.

When carrying out a similar analysis of infrasonic data, we find some interesting differences. In contrast to the case for the seismic P-waves, the azimuth scatter found by our f-k estimation process does not decrease when the array aperture increases. Furthermore, the average azimuth remains the same both with varying array aperture and with varying filter bands. This is also in contrast to what we have observed for the seismic P-waves.

In future work we plan to expand upon these studies by analyzing data from other source regions. Whe the infrasound array near ARCES becomes operational (expected in 2006), we will obtain important supplementary data to carry out such expanded studies.

References

Geller, R.J. and Mueller, C.S. (1980). Four similar earthquakes in Central California, *Geophys. Res. Lett.*, **7**, pp. 821-824.

Gibbons, S. J., Kværna, T., and Ringdal, F. (2005). Monitoring of seismic events from a specific source region using a single regional array: a case study, *J. Seism.*, **9**, pp. 277-294.

Gibbons, S. J. and Ringdal, F. (2004). A waveform correlation procedure for detecting decoupled chemical explosions, NORSAR Scientific Report: Semiannual Technical Summary No. 2 - 2004. NORSAR, Kjeller, Norway. pp. 41-50.

Gibbons, S. J. and Ringdal, F. (2005a). The detection of rockbursts at the Barentsburg coal mine, Spitsbergen, using waveform correlation on SPITS array data, NORSAR Scientific Report: Semiannual Technical Summary No. 1 - 2005. NORSAR, Kjeller, Norway. pp. 35-48.

Gibbons, S. J. and Ringdal, F. (2005b). Detection of the aftershock from the 16 August 1997 Kara Sea event using waveform correlation, NORSAR Scientific Report: Semiannual Technical Summary No. 2 - 2005. NORSAR, Kjeller, Norway, 24-31.

Kværna, T., Gibbons, S. J., Ringdal, F., and Harris, D. B. (2005). Integrated Seismic Event Detection and Location by Advanced Array Processing. In *Proceedings of the 27th Seismic Research Review, Rancho Mirage, California, September 2005. "Ground-based Nuclear Explosion Monitoring Technologies"*. pp. 927-936.

Ringdal, F., and Kværna, T. (1989). A multi-channel processing approach to real time network detection, phase association, and threshold monitoring, *Bull. seism. Soc. Am.*, **79**, pp. 1927-1940.

Schweitzer, J. and B. L. N. Kennett (2002). Comparison of Location Procedures - The Kara Sea event of 16 August 1997, NORSAR Scientific Report: Semiannual Technical Summary No. 1 - 2002. NORSAR, Kjeller, Norway. pp. 97-103.

Vinogradov, Yu. and F. Ringdal (2003). Analysis of infrasound data recorded at the Apatity array, NORSAR Scientific Report: Semiannual Technical Summary No. 1 - 2003. NORSAR, Kjeller, Norway. pp. 68-77.

Acknowledgements

This research has been supported partly under contract W9113M-05-C-0224.

Frode Ringdal
Steven J. Gibbons